Environmental Engineering and Management Journal *April 2018, Vol.17, No. 4, 783-793*
http://www.eemj.icpm.tuiasi.ro/; http://www.eemj.eu

"Gheorghe Asachi" Technical University of Iasi, Romania

KINETICS AND EQUILIBRIUM STUDIES OF 4-CHLOROPHENOL ADSORPTION ONTO MAGNETIC ACTIVATED CARBON COMPOSITES

Marius Sebastian Secula[1]*, Etelka Dávid[1], Benoît Cagnon[2], Andreea Vajda[1], Corneliu Stan[1], Ioan Mămăligă[1]

[1]"Gheorghe Asachi" Technical University of Iasi, Faculty of Chemical Engineering and Environmental Protection, 73 Prof.dr.doc. D. Mangeron, 700050 Iasi, Romania
[2]ICMN (UMR 7374 CNRS), Universited'Orleans, 1B, Rue de la Ferollerie, 45071 Orleans, France

Abstract

Among the organic pollutants, the chlorinated phenols represent an important class of compounds having a stable world market of ca. 100 kt per year. Due to their aryl structure and presence of the chlorine atom, chlorinated phenols are exceptionally recalcitrant toward chemical reactions aimed at their reduction. Adsorption from liquid phase has received special interest due to its flexibility and simplicity in operation. Especially adsorption using activated carbon (AC) has been recognized by the US Environmental Protection Agency as one of the best available control technologies due to the high surface area, large adsorption capacities and porous structure of AC.
The purpose of this study was to investigate the adsorption mechanisms of 4-chlorophenol (*4-CP*) from aqueous solutions on AC-based magnetic composites. Three different granular activated carbon materials (GAC), L27, S21 and X17, were selected based on their chemical surface properties to prepare magnetic composites through the co-precipitation method. Two kinds of composites, magnetic composites (M-L27, M-S21 and M-X17), and pre-oxidized magnetic composites (M-L27/HNO_3, M-S21/HNO_3 and M-X17/HNO_3) were tested. Significant lower values of surface area were obtained in case of pre-oxidized magnetic composites due to their higher hydrophilicity. L27-based adsorbents lead to the fastest kinetics of *4-CP* adsorption, whereas S21-based adsorbents have the highest values of adsorption capacity. The highest Fe content of 4.41% was achieved in case of M-L27 composite.

Key words: adsorption, equilibrium, kinetics, magnetic activated carbon, micropollutant

Received: May, 2017; Revised final: February, 2018; Accepted: March, 2018; Published in final edited form: April 2018

1. Introduction

Chlorophenols (CPs) are among the most persistent and hazardous organic compounds. Given their strong toxicity and resistance to biodegradation, they have been listed as persistent organic pollutants (POP) by the Clean Water Act of the US Environment Protection Authority and European Decision 2455/2001/EC) (Ajeel et al., 2015; Allaboun and Abu Al-Rub, 2016; Hwang et al., 2015; Nourmoradi et al., 2015). The major source of chlorophenol pollution is represented by the industrial discharges from petrochemical and pesticide industries and their hospital and domestic use. Chlorophenols are also generated *in-situ* during the chlorination process applied for the elimination of microbes from water (Duan et al., 2014; Lavand and Malghe, 2015). For human consumption, the limiting levels of various chlorophenols in water are below 0.1 mg/L (Aslam et al., 2015). Compared to meta- and para-chlorophenols, the ortho- substituted congeners are known to be of lower toxicity. The former substituted chlorines apparently shield the HO- group, thus having the property to interact with the available

* Author to whom all correspondence should be addressed: e-mail: mariussecula@ch.tuiasi.ro, Phone:+40 - 232 278683 / int. 2135; Fax: +40 - 232 271311

active sites from the aquatic media (Markovic et al., 2015). In particular, *p*-chlorophenol is directly relevant for water remediation due to its solubility and the severity of its threat to terrestrial and aquatic life (Nguyen and Juang, 2015).

Adsorption and advanced oxidation processes are known as highly efficient treatment methods for the removal of organic pollutants from water environments. Various adsorbents have been designed and tested for the removal of organics (Aghdam et al., 2015; Fard et al, 2017; Fard and Barkdoll, 2018). Although the adsorption process is relatively simple and involves mild operational conditions, its performance towards the removal of organic compounds is lower than that of other techniques (Irani et al., 2015). Advanced oxidation processes (AOPs) are based on the generation of highly reactive species, mainly hydroxyl radicals (HO·), which have the strongest oxidation potential, excepting fluorine (in acidic media), and are able to mineralize almost all organic compounds to carbon dioxide and water (Liu et al., 2015; Nourmoradi et al., 2015). Among AOPs, the Fenton process using a mixture of hydrogen peroxide (H_2O_2) as oxidant and ferrous iron (Fe^{2+}) as catalyst (to accelerate the degradation rate of organic compounds) has been intensively studied for environmental remediation (Chen et al., 2015; Messele et al., 2015; Yao et al., 2013). It has many advantages, such as high performance and simplicity for the oxidation of organics, mild reaction conditions (operated at room temperature and atmospheric pressure), non-toxicity (H_2O_2 can break down into environmentally safe species like H_2O and O_2) and the materials required are inexpensive (Wang M. et al., 2016; Wang N. et al., 2016).

The Fenton process consists in a transfer of electrons from a strong oxidizing agent (hydrogen peroxide) towards a transitive metal in the bulk solution, generally iron (II) (Fe^{2+}), resulting in the formation of hydroxyl radicals that attack further the organic matter (Martin del Campo et al., 2014). The chemical reaction is described by Eq. (1):

$$Fe^{2+} + H_2O_2 \rightarrow Fe^{3+} + OH^- + \bullet OH \quad (1)$$

AOPs can be also used in combinations termed *hybrid methods* such as ultrasound assisted Fenton, sonophotocatalysis, photo-Fenton, and ozone/hydrogen peroxide, in order to enhance the oxidation efficiency and overcome the limitations of individual AOPs toward some specific pollutants (Saharan et al., 2014). The combined system of UV irradiation and Fenton process, namely the photo-Fenton process, has been developed (Fard et al., 2013). This process results in a higher degree of mineralization due to the enhanced production of •OH radicals. In this case, hydroxyl radicals are generated due to both the photo-decomposition of hydrogen peroxide and iron catalyzed decomposition (Eq. 2) (Bel Hadjltaief et al., 2014).

$$H_2O_2 + UV \rightarrow \bullet OH + \bullet OH \quad (2)$$

In particular, iron oxide nanoparticles represent a promising adsorbent due to their high reactivity; moreover, elemental iron is non-toxic and ubiquitous on Earth (accounting for 6% wt. of the Earth's crust) (Xu et al., 2013).

Considering the excellent adsorption capacity of activated carbon, many studies have been focusing on the development of novel adsorbents that combine the adsorption capacity of carbon materials with the magnetic properties of iron oxides (Istratie et al., 2016).

In the present study, a combined adsorption and Fenton oxidation method is proposed using granular activated carbons as starting materials. The ACs were modified by chemical treatment in order to obtain supports with different surface chemistry. The co-precipitation method was employed to prepare iron-impregnated catalysts on different activated carbon supports, and applied in the photo-Fenton-like degradation process of *4-CP*.

The adsorption step of the treatment process allows *4-CP* to be immobilized and concentrated on the activated carbon surface and when Fenton oxidation is carried out the degradation of the adsorbate is much more efficient and effective compared to chemical oxidative processes carried out in the dilute solution (Kim et al., 2015).

The main objective of this study was to develop and compare the performance of raw activated carbons having different surface properties, magnetic and pre-oxidized magnetic activated carbons applied further for the removal method of *4-CP* from water by adsorption and photo-Fenton processes.

The physical and chemical properties of GAC composites were analyzed and the catalytic performances were assessed according to the effects of some key parameters, such as initial value of solution pH, phenol initial concentration, and contact time. The reaction kinetics, isotherms, material stability and degradation mechanism were evaluated.

Experimental data on the desorption of *4-CP* from GAC by NaOH and Et-OH solutions are also presented and discussed.

2. Material and methods

2.1. Material

Activated carbon materials were acquired from PICA-Jacobi (France). Three types of ACs, L27, S21 and X17, were employed in this study in order to establish the influence of surface pH_{PZC}on the performance of the achieved Fenton-like catalysts. Before use, the ACs were washed for 24 h with bidistilled water to eliminate the residual acidity or basicity, and then dried at 75°C for 24 h. The *4-CP* (>99.5%), HNO_3 (65%), ferrous sulfate heptahydrate (>99%), iron(III) nitrate nonahydrate (≥98%), ammonium hydroxide, ethanol (97%) and hydrogen peroxide were purchased from Sigma Aldrich and used without further purification. All solutions were prepared using bidistilled water.

2.2. Preparation of acid treated Fe-amended activated carbon

The ACs were used either as such (to prepare magnetic GACs) or each of the adsorbents was oxidized with concentrated HNO_3 (pre-oxidized GACs) in an ultrasonic bath (GFL 1092) for 60 min, washed with bidistilled water and dried. The active metal was supported on activated carbons by co-precipitation of $FeSO_4 \cdot 7H_2O$ and $Fe(NO_3)_3 \cdot 9H_2O$. The magnetic composites were prepared by contacting 3 g of raw and oxidized ACs respectively with the solution of precursors with a calculated concentration. The resulting mixture was sonicated for 15 min at room temperature. 8 M ammonium hydroxide solution was added dropwise to adjust the pH to 12 in order to precipitate Fe_3O_4. This reaction was conducted for 1 h at 50°C under mechanical stirring. After impregnation, the samples were rinsed and dried at 55°C in an oven. Two types of composites were obtained: magnetic composites and pre-oxidized magnetic composites denoted here in further as M-L27, M-S21, M-X17 and M-L27/HNO_3, M-S21/HNO_3, M-X17/HNO_3 respectively.

2.3. Characterization methods

Textural characterization of the supports and catalysts was performed by means of the N_2 adsorption-desorption isotherms, recorded at 77 K using an ASAP 2020 (Micromeritics Inc., USA). The pore size distribution was determined by the Density Functional Theory (DFT) method (function provided by Micromeritics software). Thermogravimetric analyses (TG/DTG) were recorded on Thermogravimetric analysis (TGA 92 Setaram) in the temperature range of 21 - 1000°C. Fourier transform infrared (FTIR) spectra of the complexes were recorded using a Perkin Elmer Spectrum 100 spectrometer over a wavenumber range of 4000–400 cm^{-1} and the conventional KBr pellet method. Total iron content in the obtained composites and iron leakage were determined by spectrophotometry using phenantroline method (Clesceri et al., 1989). The concentration of *4-CP* was determined using a UV–Vis Hitachi 5100 spectrophotometer at the maximum specific wavelength of 223 nm.

2.4. Adsorption-desorption experiments

The adsorption experiments were performed in batch mode with the aid of an orbital shaker. The initial concentration was varied between 20-250 mg/L. An adsorbent mass of 0.1 g was added to 250 mL glass flasks filled with 250 mL of adsorbate solution of known initial concentration and shaken for 24h. In the kinetics tests, samples of 4 mL were systematically taken at appropriate time intervals using a syringe. Then, they were separated by centrifugation and then 1mL was diluted and analyzed spectrophotometrically. The desorption runs were carried out also in batch mode. Certain weights of spent adsorbents were added to 50 mL bidistilled water and samples were taken after the equilibrium has been established.

The performance of the synthesized catalysts was evaluated in Fenton and photo-Fenton processes of *4-CP* degradation. Catalytic degradation experiments were carried out for 2h in conical flasks, on a magnetic stirrer using a catalyst dosage of 0.1 g/250 mL *4-CP* solution, pH of 3, H_2O_2 concentration of 100 mg/L. Photo-catalytic oxidation was conducted under the irradiation of a Pen-Ray-Power Supply lamp (UVP Products, TQ 718, and 700 W) at 312 nm and at room temperature.4 mL of reaction mixture were systematically sampled, separated by centrifugation and then 1mL was diluted and analyzed by means of a UV-Vis spectrophotometer following absorbance at the maximum wavelength of *4-CP*, 280 nm. After analysis, the undiluted solution was added back into the photocatalytic reactor to minimize the loss in total volume and maintain the solid/liquid ratio.

The amount of solute adsorbed at time *t*, q_t (mg/g) and at equilibrium state, q_e (mg/g) were calculated according to the following equations (Eqs. 3-4):

$$q_t = (C_0 - C_t)\frac{V}{m} \quad (3)$$

$$q_e = (C_0 - C_e)\frac{V}{m} \quad (4)$$

where: C_0 is the initial concentration of the adsorbate (mg/L); C_t and C_e are the concentration of *4-CP* in solution at equilibrium and at time *t* (mg/L); *V* is the volume of the aqueous solution (L); *m* is the mass of adsorbent (g).

2.5. Kinetic models

The *4-CP* adsorption kinetics data were fitted with the linearized form of the following three adsorption models:

- pseudo-first-order kinetic model (Lagergren and Svenska, 1898) (Eq. 5):

$$log(q_e - q_t) = log\, q_e - k_1\, t \quad (5)$$

- pseudo-second-order kinetic model(Ho and McKay, 1998) (Eq. 6):

$$\frac{t}{q_t} = \frac{1}{k_2 q_e^2} + \frac{t}{q_e} \quad (6)$$

where: q_e and q_t are the adsorption capacities at equilibrium and at time *t*, respectively (mg g^{-1}); k_1 is the rate constant of pseudo-first-order adsorption (L min^{-1}); k_2 is the rate constant of pseudo-second-order adsorption (g $(mg \cdot min)^{-1}$).

- intraparticle diffusion model (Weber and Morris, 1963) (Eq. 7):

$$q_t = K_{dif} \cdot t^{0.5} + I \quad (7)$$

where: K_{dif} is the intraparticle diffusion rate constant (mg (g $h^{0.5})^{-1}$); I indicates the thickness of the boundary layer diffusion (mg g^{-1}).

2.6. Adsorption isotherms

The experimental data on adsorption were analyzed using Langmuir, Freundlich, and Dubinin Radushkevich (DR) isotherm models. The theoretical form of the Langmuir isotherm is given by the following equation (Langmuir, 1916) (Eq. 8):

$$q_e = \frac{Q_{max} K_L C_e}{1+K_L C_e} \quad (8)$$

where: Q_{max} is the maximum adsorption capacity (mg g^{-1}); K_L is a constant related to the adsorption free energy (L mg^{-1}).

The essential characteristics of the Langmuir isotherm can be expressed by the separation factor (a dimensionless constant), R_L, which is expressed as (Eq. 9):

$$R_L = \frac{1}{1+K_L C_0} \quad (9)$$

When the R_L value is zero the adsorption process is irreversible, if it one, the adsorption is linear, and if R_L takes values between zero and one, the adsorption is favorable.

The Freundlich isotherm is given by Eq. (10) (Freundlich, 1906):

$$q_e = K_F C_e^{1/n} \quad (10)$$

where: K_F (L mg^{-1}) is Freundlich constant related to the adsorption capacity; n is a constant related to the adsorption intensity. When n>1, it means the adsorption conditions for are favorable.

The third isotherm investigated within this study was the Dubinin–Raduchkevitch (DR) isotherm which is used to estimate the nature of the adsorption process (physical or chemical). It is described by the following relation (Dubinin et al., 1947) (Eq. 11):

$$lnq_e = lnq_m - K_{ads}\varepsilon^2 \quad (11)$$

where: q_e is the uptake at equilibrium(mgg^{-1}); K_{ads} is the adsorption energy constant (J^2mol^{-2}); ε is the Polanyi potential defined by (Eq. 12):

$$\varepsilon = RT\, ln\left(1+\frac{1}{C_e}\right) \quad (12)$$

where: R is the gas constant (8.314 J/(mol K)) and T is the absolute temperature.

Describing the nature of the adsorption, the value of the adsorption energy (E), which indicates the, was determined through Eq. (13) (Barkat et al., 2015):

$$E = \frac{1}{\sqrt{2K_{ads}}} \quad (13)$$

A value of E less than 8 kJ/mol points out a physical adsorption, an E value between 8 and 25 kJ/mol shows a chemical ion exchange process, and if it is higher than 25 kJ/mol it involves chemical adsorption.

3. Results and discussion

3.1. Characterization of adsorbents

The raw ACs (L27, S21 and X17) have different porous properties. The N_2 adsorption-desorption isotherms showed that L27 and X17 were microporous but also contained some mesopores while S21 was microporous only, which was confirmed by the values of its S_{micro} and S_{ext}. L27 AC is acidic, S21, neutral and X17, basic. Table 1 summarizes the textural properties of the ACs based on N_2 isotherms. The N_2 adsorption-desorption isotherms recorded for M-L27 (figure not shown) showed an enlarged hysteresis loop compared to raw L27, indicating an increased mesopore volume, confirmed by the increased mean pore size. For the oxidized M-L27 the adsorbed volume decreased even more pronounced. Before each N_2 isotherm, a degassing step was conducted for 24 h at 250°C and 4 μm Hg, and the mass loss corresponds to water evaporation. The determined values of water loss are shown in Table 2.

Table 1. Textural properties of the raw and magnetic GACs

AC	V_{micro}(cm^3g^{-1})	L_0 (Å)	S_{ext} (m^2g^{-1})	S_{micro} (m^2g^{-1})	S_{total} (m^2g^{-1})
L27	0.57	18.5	444	616	1060
M-L27	0.46	25.4	644	362	1006
M-L27/HNO_3	0.38	17.2	492	442	934
S21	0.47	9.7	18	969	987
M-S21	0.06	19.5	12	62	74
M-S21/HNO_3	0.30	8.3	23	723	746
X17	0.29	15.1	130	382	514
M-X17	0.28	15.0	145	373	518
M-X17/HNO_3	0.26	13.7	155	380	535

Table 2. Water loss of magnetic GACs

GAC	*M-L27*	*M-L27/HNO₃*	*M-S21*	*M-S21/HNO₃*	*M-X17*	*M-X17/HNO₃*
Water loss (%)	5.6	11.4	4.0	6.8	4.2	8.2

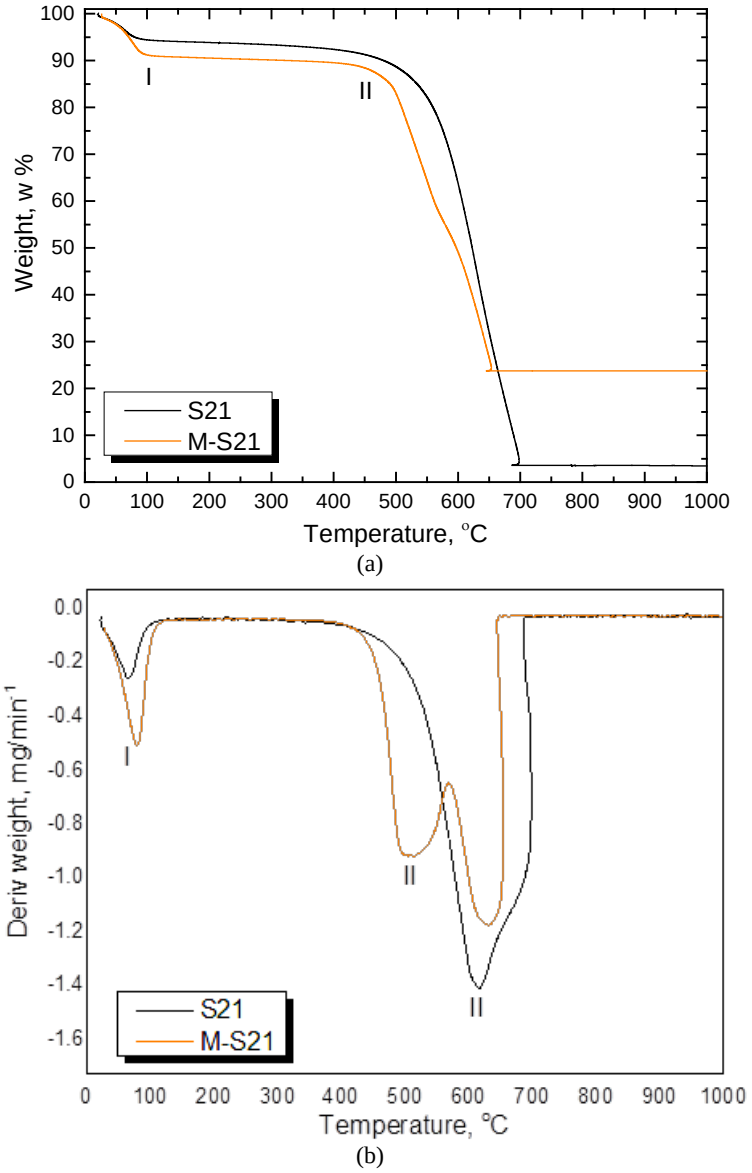

Fig. 1. TG and DTG curves of S21 (a) and M-S21 (b)

In case of the magnetic composites prepared on the support S21, characterized by microporosity, a strong decrease in the microporous volume was observed, caused by pore-clogging due to the impregnation with iron oxides, resulting in a decrease of the total surface area. For X17 and M-X17 it was observed a significant increase in the pores similar in size to the *4-CP* molecule (6.47×4.17 Å). However, the change in porous structure appears to be less important in case of X17 in comparison with those noticed in case of L27 and S21.

The decreased surface area of the pre-oxidized magnetic composites may be due to the high amount of oxygen-containing groups introduced on the AC surface with HNO_3 treatment, which may block the entry of N_2 molecules inside the small pores (Chen et al., 2015).

Thermogravimetric analysis was employed in order to determine the main decomposition stages of raw and composite GACs. Since all the ACs showed similar behavior, Fig. 1 presents the TG of S21 and M-S21 only. The shape of the thermal curves is similar for the two types of adsorbents, which exhibit only two decomposition stages: one up to 100°C, which corresponds to the dry AC, while stage II, in the range 500-600°C, corresponds to a carbonized material showing a slower deconstruction of the magnetic composite compared to that of raw AC. The residual weight of S21 and M-S21 points out the presence of iron oxides in the magnetic composites.

Total iron content was determined by using phenanthroline spectrophotometric method. The results showed that the iron content in the Fe-GAC magnetic composites decreased in the following order: magnetic L27>S21>X17 (Fig. 2). Thus M-L27 has the highest total iron content (4.41%) while X17 is expected to be less suitable as a catalyst support for Fe_3O_4 (Bayazit and Kerkez, 2014) as it has the lowest total iron content. However, M-GACs have proven to have a higher total iron content than those activated with HNO_3.

Fig. 3 exemplifies the case for S21. This AC has no surface oxygen groups. HNO_3 activation increases the hydrophilicity of magnetic GACs as emphasized by the peaks at 3423 and 3491 cm^{-1}. The spectrum of M-S21/HNO_3 shows peaks at 1510, 1710 which are characteristics of carboxylic groups.

Both the FTIR spectra and the water loss data (after drying the GACs) point out that the pre-oxidized carbons are more hydrophilic, suggesting that HNO_3 activation increases the hydrophilicity of magnetic GACs. Therefore, it is expected a relatively lower adsorption capacity of these adsorbents.

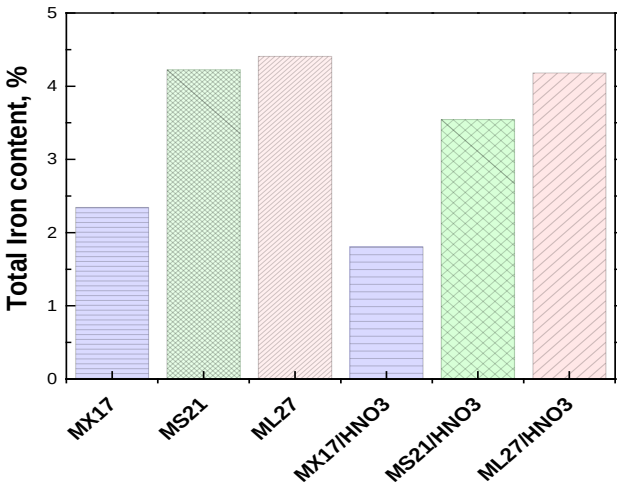

Fig. 2. Total Iron content in synthesized Magnetic GACs

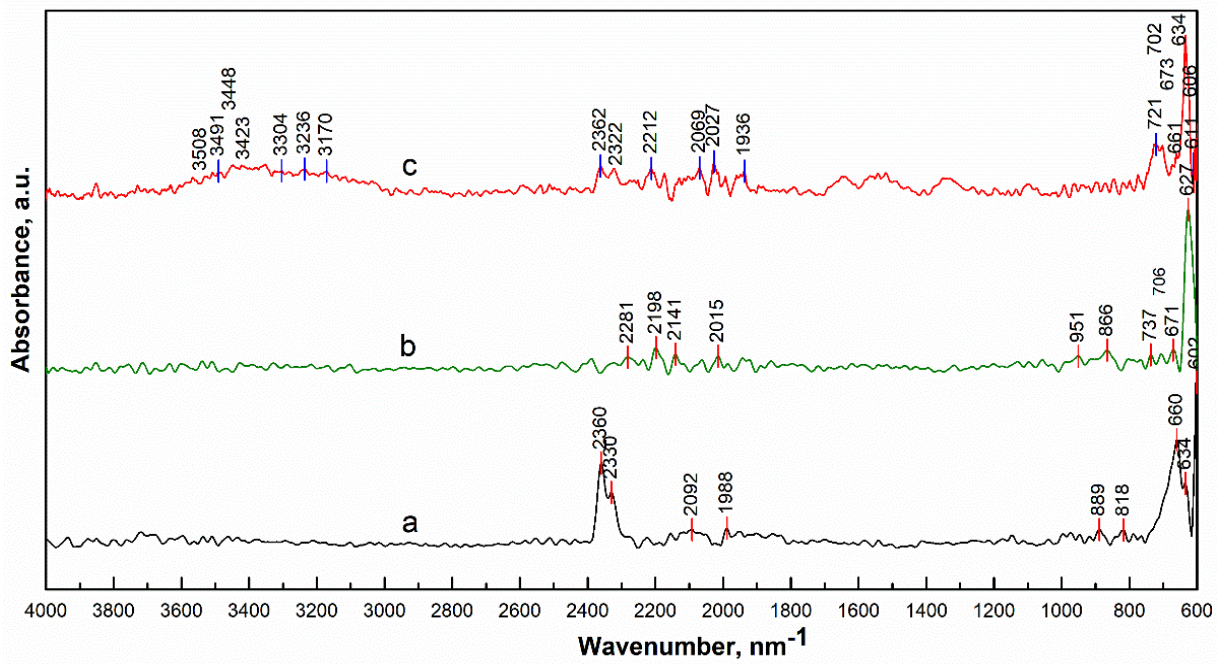

Fig. 3. FTIR spectra of raw and magnetic S21: a. S21, b. M-S21, c. M-S21/HNO_3

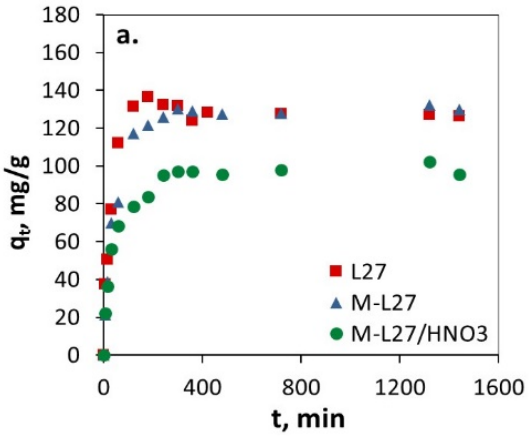

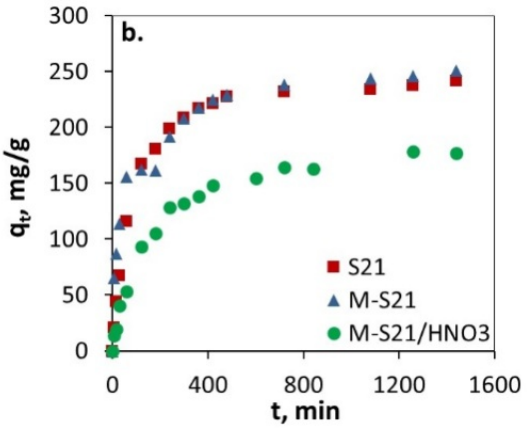

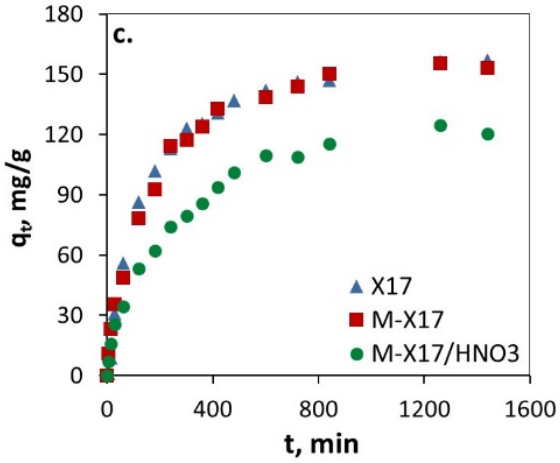

Fig. 4. Amount of *4-CP* adsorbed as a function of contact time (C_0 = 100 mg/L, 0.1 g CA)

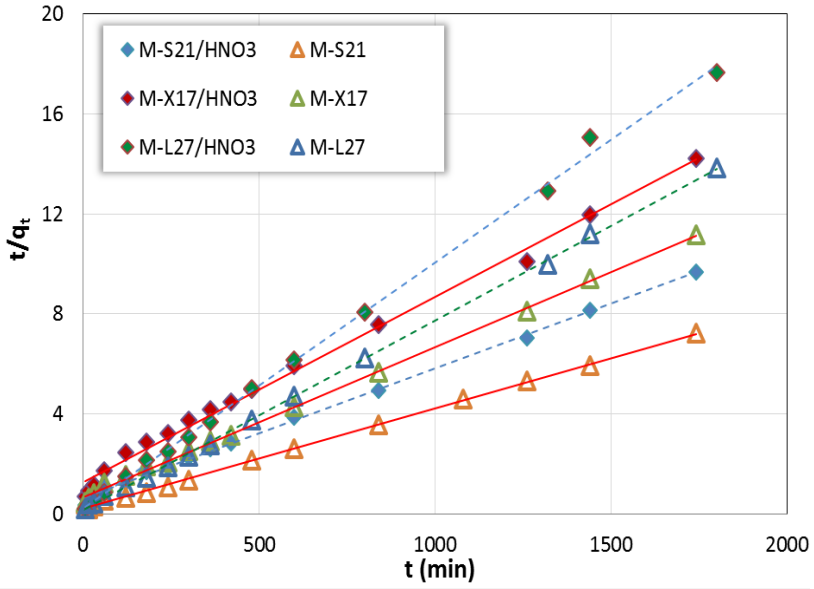

Fig. 5. Pseudo-second-order kinetic plots for adsorption of *4-CP* onto magnetic AC

3.2. Effect of contact time

The time dependence for *4-CP* adsorption onto the activated carbons modified with HNO_3 and iron salts was investigated to determine the time needed to reach the equilibrium. The experimental data are plotted as adsorbed amounts versus contact time (Fig. 4).

As shown in Fig. 4, *4-CP* adsorption was quite fast in the first 2h, then gradually increased with the extended contact time. After 12h of contact time, no obvious variation in the amounts of *4-CP* adsorbed was noted. The raw and magnetic carbons had a similar adsorption behavior toward *4-CP*, the main difference being the adsorption capacity of M-X17 which decreased slightly due to alteration of the microporous matrix after impregnation with iron. As regards the pre-oxidized magnetic composites, the figures show a significant decrease in adsorption capacity. This phenomenon was already reported by Messele et al. (2015) who suggested that water forms hydrogen bonds with the hydrophilic oxygenated groups present on the carbon surface, resulting in clusters that can block the passage of phenolic molecules to the surface. It is worth mentioning also that the solubility of *4-CP* (26 g/L) is significantly lower than that of phenol (76 g/L) so there is a competition between water and *4-CP*.

3.3. Kinetic models and adsorption mechanism

Generally, kinetic models are employed to determine the rate of the adsorption process (Ahmed and Theydan, 2013). Three kinetic models - pseudo-first order, pseudo-second order and intraparticle diffusion- were used to correlate the experimental kinetic data.

Table 3 shows the values of kinetic parameters for 4-CP adsorption onto the considered adsorbents. There is a high deviation between the experimental and calculated adsorption capacity for the pseudo-first order model, which reflects the poor fitting of this model to the experimental data. Moreover, the pseudo-first order had low R^2 values, whereas for the pseudo-second order equation the correlation of the linear plot between *t/qt* and *t* (Fig. 5) has high R^2 values (Table 3).

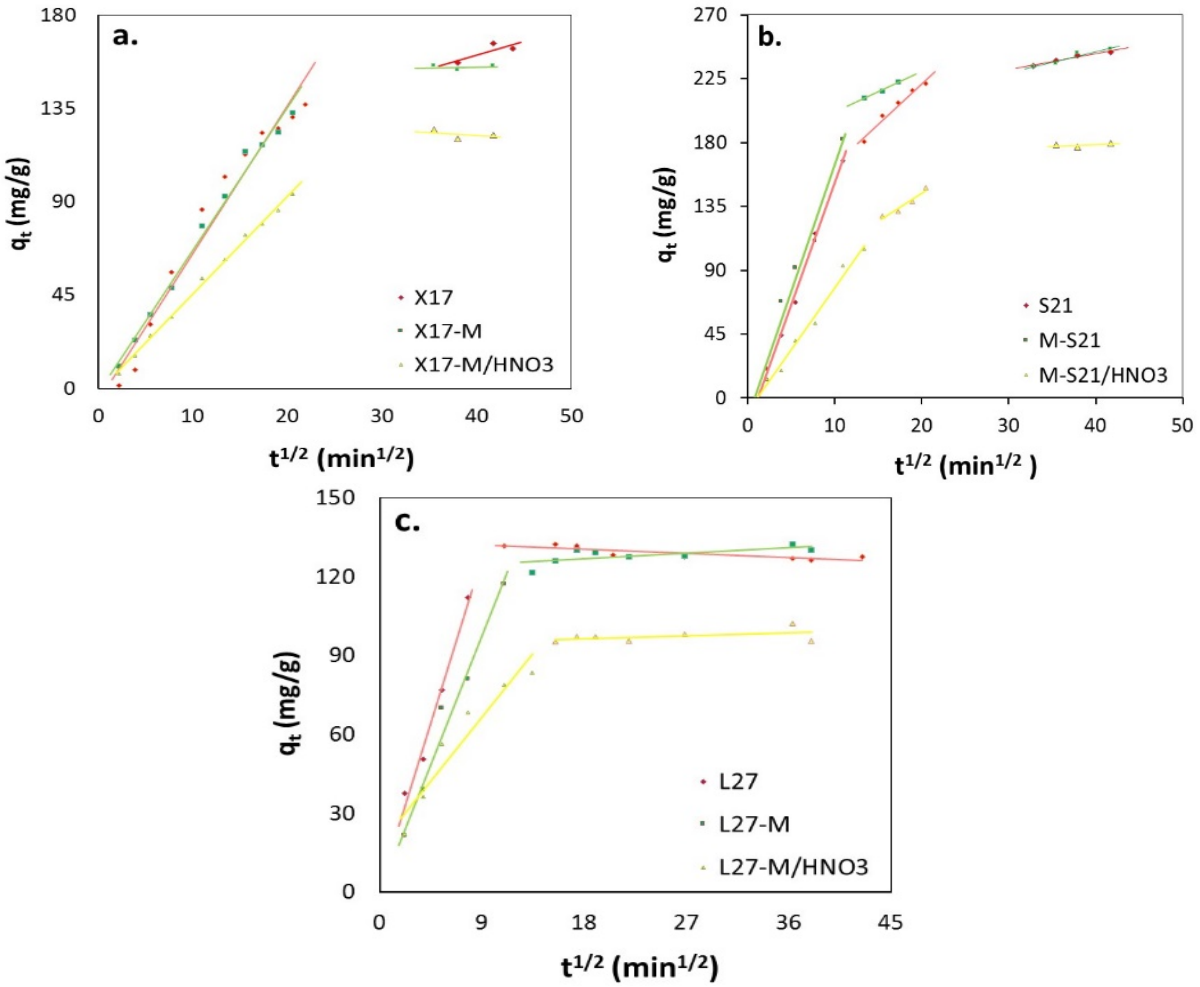

Fig. 6. Adsorption of 100 mg/L *4-CP* onto raw and magnetic AC

Table 3. Kinetic parameters for *4-CP* adsorption onto raw and magnetic activated carbons

AC	q_{exp} (mg/g)	*Pseudo-first-order*			*Pseudo-second-order*			*Intraparticle diffusion*		
		q_{calc} (mg/g)	k_1 (h^{-1})	R^2	q_{calc} (mg/g)	k_2 (g/(mg h))	R^2	K_{dif} (mg/(g $h^{1/2}$))	I (mg/g)	R^2
L27	127.60	123.18	0.027	0.998	127.62	0.0016	0.999	13.851	2.388	0.983
								-0.18	133.78	0.770
M-L27	129.99	71.08	0.008	0.816	132.16	0.0004	0.999	10.108	3.161	0.965
								0.209	123.09	0.383
M-L27/HNO_3	101.99	54.05	0.006	0.838	101.82	0.0004	0.998	5.416	-18.099	0.909
								0.122	94.184	0.217
S21	246.54	114.69	0.002	0.906	252.45	$6.103 \cdot 10^{-5}$	0.999	17.224	-21.388	0.996
								5.730	107.33	0.965
								0.962	512.173	0.989
M-S21	242.96	104.67	0.002	0.813	249.08	$7.533 \cdot 10^{-5}$	0.998	17.896	-15.472	0.962
								1.427	194.416	0.799
								1.392	188.229	0.916
M-S21/HNO_3	179.51	138.86	0.003	0.956	193.03	$4.089 \cdot 10^{-5}$	0.998	8.754	-9.651	0.983
								3.954	65.209	0.942
								0.225	169.60	0.272
X17	201.72	131.25	0.001	0.798	205.76	$1.074 \cdot 10^{-5}$	0.967	10.197	-25.024	0.990
								3.923	51.543	0.973
								0.870	128.222	0.977
M-X17	155.76	137.57	0.004	0.988	166.57	$5.206 \cdot 10^{-5}$	0.999	7.571	-6.517	0.994
								5.133	28.253	0.926
								0.088	151.48	0.041
M-X17/HNO_3	122.37	111.48	0.003	0.993	134.95	$4.414 \cdot 10^{-5}$	0.995	4.715	-1.966	0.998

Table 4. Isotherm constants and correlation coefficients for adsorption of *4-CP* onto AC

AC	*Langmuir*				*Freundlich*			*Dubinin-Radushkevich*			
	K_L (L/mg)	b (mg/g)	R_L	R^2	K_F	n	R^2	K_{ads}x10^{-9}	q_m (mg/g)	E (kJ/mol)	R^2
L27	0.028	236.71	0.320	**0.981**	23.920	2.360	0.943	4.810	793.27	10.190	0.960
M-L27	0.028	261.98	0.319	0.914	32.633	2.647	0.982	3.510	550.84	11.942	**0.988**
M-L27/HNO$_3$	0.064	115.53	0.120	0.954	30.623	3.928	0.974	2.765	238.03	13.448	**0.983**
S21	1.276	295.09	0.009	0.912	154.83	6.026	0.957	1.533	551.56	18.061	**0.990**
M-S21	0.112	292.00	0.118	**0.965**	111.27	5.263	0.847	2.890	681.40	13.162	0.869
M-S21/HNO$_3$	0.157	214.06	0.089	**0.996**	80.46	4.964	0.917	2.530	463.82	14.058	0.894
X17	0.209	194.97	0.069	**0.995**	81.933	5.486	0.901	2.500	439.56	14.146	0.938
M-X17	0.139	190.15	0.107	0.968	53.278	3.380	0.992	2.712	467.75	13.578	**0.994**
M-X17/HNO$_3$	0.057	128.42	0.218	0.969	29.867	3.579	0.989	3.094	278.51	12.713	**0.995**

The results listed in Table 3 show that the adsorption kinetic data are better represented by the pseudo-second order model and the calculated values (q_{calc}) agree well with the experimental ones (q_{exp}). This indicates the second-order kinetics for *4-CP* adsorption on the studied carbons, suggesting that adsorption depends on the adsorbate as well as the adsorbent and involves chemical reaction as a rate controlling parameter, in addition to physisorption (Goscianska et al., 2015; Mohd et al., 2009).

The curve-fitting plots of the intraparticle diffusion model are presented in Fig. 6 at 25°C. In case of raw and magnetic X17 and L27 the adsorption process can be divided in two regions: the first one, sharper portion is attributed to the external surface adsorption and the second plateau portion corresponds to the final equilibrium process when intraparticle diffusion starts to slow down due to extremely low solute concentrations in the solution.

The existence of an external layer diffusion process can be inferred because these plots do not pass through the origin (Liu et al., 2010). Between the sharp rise and the plateau portion, a less steep stage is observed for the composite adsorbents based on S21. The second region corresponds, in this case, to the gradual adsorption stage when diffusion is restricted mainly by the microporous structure of the ACs. The third portion is the final equilibrium stage where diffusion is retarded by the formerly adsorbed molecules. The I values for all the ACs indicate that intraparticle diffusion is not the only rate-limiting step in the sorption process.

3.4. Equilibrium models

An adsorption isotherm is commonly depicted by expressing graphically the unit mass of solid-phase against the solute equilibrium concentration. Three widely used models, Langmuir, Freundlich and Dubinin-Radushkevich, were applied for the fitting of the experimental data. Table 4 indicates the sorption isotherms parameters. The adsorption of *4-CP* on magnetic L27 and X17 composites is best described by the Dubinin-Radushkevich model, whereas that based on S21 fits the Langmuir model better in terms of determination coefficients. The n value obtained from the Freundlich isotherm was more than one, suggesting that the uptake of *4-CP* was suitably accomplished by all the adsorbents. The adsorption energy, E, calculated from the adsorption energy constant, ranged between 10.19 and 18.06 kJ/mol, clearly indicating a chemical ion exchange mechanism.

3.5. Fenton and photo-Fenton degradation of 4-CP

Several batch experiments were performed to assess the catalytic ability of magnetic GACs toward *4-CP* degradation in presence of H_2O_2. Among the different catalysts used in heterogeneous Fenton-like reactions, Fe containing carbons have shown high catalytic activities in the oxidation of organic compounds, with minimal iron leaching and easy recovery. The studies showed that M-L27, beside its highest Fe content, has the fastest adsorption kinetics in relation to *4-CP* among all the synthesized composites.

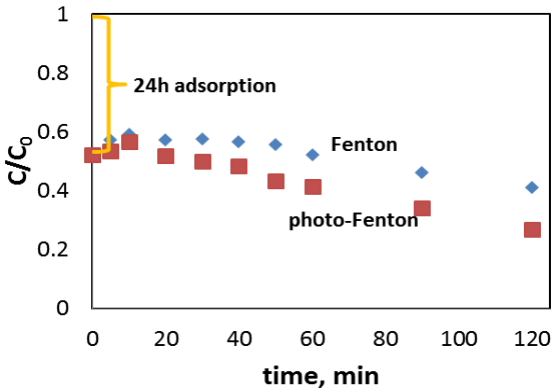

Fig. 7. Degradation and photo-degradation of *4-CP* by heterogeneous Fenton, (100 mg/L *4-CP*, 0.4 g/L M-L27, 100 mg/L H_2O_2)

Therefore, before the AOP tests, M-L27 previously saturated with *4-CP* was subjected to the oxidation process. Fig. 7 shows the measured 4-CP degradation performance by Fenton and photo-Fenton oxidation as a function of reaction time. The results show an increase in *4-CP* concentration in the first hour of the Fenton reaction which can be explained by

4-CP desorption from the M-L27 surface. However, the degradation process starts as the catalyst surface is unloaded. UV irradiation also seems to be an important feature for achieving higher *4-CP* removal efficiencies.

3.6. Desorption studies

The feasibility of regenerating the spent activated carbon saturated with *4-CP* was evaluated. The effect of ultrasound and agitation on the desorption of *4-CP* from the spent magnetic ACs using solutions of NaOH and Et-OH (ethyl alcohol) were evaluated and compared. For this purpose, a volume of 50 mL of ethyl alcohol or 20% NaOH solution, respectively were added to the desorption system in the presence of sonication for 2h, or agitation for 24h, at room temperature.

The results presented in Fig. 8 emphasize that *4-CP* desorption significantly increased in the presence of ultrasound and ethanol solution. According to iron leakage studies, sonication and NaOH solutions are detrimental to magnetic composites. Therefore, ethanol and agitation are recommended for the desorption of *4-CP* in order to minimize the leakage of iron from the magnetic composites.

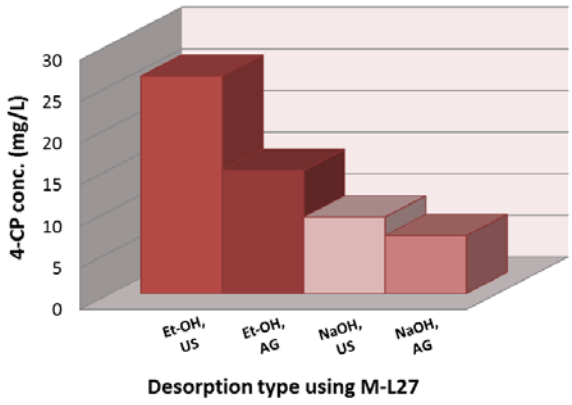

Fig. 8. Effect of agitation and stripping solution type on the desorption of *4-CP*

4. Conclusions

The adsorption mechanisms and Fenton oxidation of *4-CP* from aqueous solutions on magnetic composites were studied. Total iron content in M-GAC was higher than in the pre-oxidized magnetic composites. M-L27 had the highest iron content.

Adsorption experimental data showed a better fit with the pseudo-second-order kinetic model as indicated by higher values of the correlation coefficient. The incorporation of iron decreased the sorption capacity of X17 and S21 for *4-CP* due to alteration of the porous structure.

HNO_3 preactivation resulted in an increase in hydrophilicity and consequently in a significant decrease in the sorption capacity.

Adsorption of *4-CP* on the Magnetic X17 composite was best described by the Dubinin-Radushkevich model, magnetic L27 by the Freundlich model whereas that obtained on S21 composites was best described by the Langmuir model.

Among all the synthetized adsorbents, only M-L27 and M-L27/HNO_3 were suitable for Fenton and photo-Fenton reactions. The optimal desorption of *4-CP* was obtained under agitation in ethanol solutions.

Acknowledgements

This work was supported by a grant from the Romanian National Authority for Scientific Research and Innovation, CNCS - UEFISCDI, project number PN-II-RU-TE-2014-4-0405.

References

Aghdam E., Aminzadeh B., Baghdadi M., Fard M.A., (2015), Removal of BTEX from aqueous solutions by paper mill sludge-based activated carbon, *Journal of Advances in Chemistry*, **11**, 3416-3432.

Ahmed M.J., Theydan S.K., (2013), Adsorption of p-chlorophenol onto microporous activated carbon from Albizialebbeck seed pods by one-step microwave assisted activation, *Journal of Analytical and Applied Pyrolysis*, **100**, 253-260.

Ajeel M.A., Aroua M.K., Wan Daud W.M.A., (2015), Anodic degradation of 2-chlorophenol by carbon black diamond and activated carbon composite electrodes, *Electrochimica Acta*, **180**, 22-28.

Allaboun H., Abu Al-Rub F.A., (2016), Removal of 4-chlorophenol from contaminated water using activated carbon from dried date pits: equilibrium, kinetics, and thermodynamics analyses, *Materials*, **9**, 1-15.

Aslam M., Soomro M.T., Ismail I.M.I., Salah N., Gondal M.A., Hameed A., (2015), Sunlight mediated removal of chlorophenols over tungsten supported ZnO: Electrochemical and photocatalytic studies, *Journal of Environmental Chemical Engineering*, **3**, 1901-1911.

Barkat M., Nibou D., Amokrane S., Chegrouche S., Mellah A., (2015), Uranium (VI) adsorption on synthesized 4A and P1 zeolites: Equilibrium, kinetic, and thermodynamic studies, *Comptes Rendus Chimie*, **18**, 261-269.

Bayazit Ş.S, Kerkez Ö., (2014), Hexavalent chromium adsorption on superparamagnetic multi-wall carbon nanotubes and activated carbon composites, *Chemical Engineering Research and Design*, **92**, 20725-2733.

Bel Hadjltaief H., Da Costa P., Beaunier P., Gálvez M.E., Ben Zina M., (2014), Fe-clay-plate as a heterogeneous catalyst in photo-Fenton oxidation of phenol as probe molecule for water treatment, *Applied Clay Science*, **91-92**, 46-54.

Chen H., Zhang L., Zeng H., Yin D., Zhai Q., Zhao X., Li J., (2015), Highly active iron-containing silicotungstate catalyst for heterogeneous Fenton oxidation of 4-chlorophenol, *Journal of Molecular Catalysis A: Chemical*, **406**,72-77.

Clesceri L.S., Greenberg A.E., Trussell R.R., (1989), *WEF Standard Methods for the Examination of Water and Wastewater*, Method 3500-Fe D, Phenanthroline Method, 17th Edition, APHA, AWWA.

Duan F., Yang Y., Li Y., Hongbin C., Yi W., Yi Z., (2014), Heterogeneous Fenton-like degradation of 4-chlorophenol using iron/ordered mesoporous carbon

catalyst, *Journal of Environmental Sciences*, **26**, 1171-1179.

Dubinin M.M., Zaverina E.D., Radushkevich L.V., (1947), Sorption and structure of active carbon I. Adsorption of organic vapors, *Journal of Physical Chemistry A*, **21**, 1351-1362.

Fard M.A., Torabian A., Bidhendi G.R.N., Aminzadeh B., (2013), Fenton and photo-Fenton oxidation of petroleum aromatic hydrocarbons using nanoscale zero-valent iron, *Journal of Environmental Engineering*, **139**, 966-974.

Fard M.A., Vosoogh A., Barkdoll B., Aminzadeh B., (2017), Using polymer coated nanoparticles for adsorption of micropollutants from water, *Colloids and Surfaces A: Physicochemical and Engineering Aspects*, **531**, 189-97.

Fard M.A., Barkdoll B., (2018), Using recyclable magnetic carbon nanotube to remove micropollutants from aqueous solutions, *Journal of Molecular Liquids*, **249**(Supplement C), 193-202.

Freundlich H.M.F., (1906), About the adsorption in liquids (in German), *Zeitschriftfür Physikalische Chemie*, **57**, 385-470.

Goscianska J., Ptaszkowska M., Pietrzak R., (2015), Equilibrium and kinetic studies of chromotrope 2R adsorption onto ordered mesoporous carbons modified with lanthanum, *Chemical Engineering Journal*, **270**, 140-149.

Ho Y.S., McKay G., (1998), A comparison of chemisorption kinetic models applied to pollutant removal on various sorbents, *Process Safety and Environmental Protection*, **76**, 332-340.

Hwang Y., Mines P.D., Jakobsen M.H., Andersen H.R., (2015), Simple colorimetric assay for dehalogenation reactivity of nanoscale zero-valent iron using 4-chlorophenol, *Applied Catalysis B: Environmental*, **166-167**, 18-24.

Irani M., Roshanfekr Rad L., Pourahmad H., Haririan I., (2015), Optimization of the combined adsorption/photo-Fenton method for the simultaneous removal of phenol and paracetamol in a binary system, *Microporous and Mesoporous Materials*, **206**, 1-7.

Istratie R., Stoia M., Pacurariu C., Locovei C., (2016), Single and simultaneous adsorption of methyl orange and phenol onto magnetic iron oxide/carbon Nanocomposites, *Arabian Journal of Chemistry*, In press, Doi.org/10.1016/j.arabjc.2015.12.012.

Kim J.R., Huling S.G., Kan E., (2015), Effects of temperature on adsorption and oxidative degradation of bisphenol A in an acid-treated iron-amended granular activated carbon, *Chemical Engineering Journal*, **262**, 1260-1267.

Lagergren S., Svenska B.K., (1898), Theory of the so-called adsorption solutes (in German), *Vetenskapsakademiens Handlingar*, **24**, 1-39.

Langmuir I., (1916), The constitution and fundamental properties of solids and liquids, *Journal of the American Chemical Society*, **38**, 2221-2295.

Lavand A.B., Malghe Y.S., (2015), Visible light photocatalytic degradation of 4-chlorophenol using C/ZnO/CdS nanocomposite, *Journal of Saudi Chemical Society*, **19**, 471-478.

Liu J., Zhao Z., Shao P., Cui F., (2015), Activation of peroxymonosulfate with magnetic Fe_3O_4–MnO_2 core-shell nanocomposites for 4-chlorophenol degradation, *Chemical Engineering Journal*, **262**, 854-861.

Liu Q.-S., Zheng T., Wang P., Jiang J.-P., Li N., (2010), Adsorption isotherm, kinetic and mechanism studies of some substituted phenols on activated carbon fibres, *Chemical Engineering Journal*, **157**, 348-356.

Markovic M.D., Dojcinovic B.P., Obradovic B.M., Nešic J., Natic M.M., Tosti T.B., Kuraica M.M., Manojlovic D.D., (2015), Degradation and detoxification of the 4-chlorophenol by non-thermal plasma-influence of homogeneous catalysts, *Separation and Purification Technology*, **154**, 246-254.

Martin del Campo E., Romero R., Roa G., Peralta-Reyes E., Espino-Valencia J., Natividad R., (2014), Photo-Fenton oxidation of phenolic compounds catalyzed by iron-PILC, *Fuel*, **138**, 149-155.

Messele S.A., Soares O.S.G.P., Órfão J.J.M., Bengoa C., Stüber F., Fortuny A., Fabregat A., Font J., (2015), Effect of activated carbon surface chemistry on the activity of ZVI/AC catalysts for Fenton-like oxidation of phenol, *Catalysis Today*, **240**, 73-79.

Mohd Din A.T., Hameed B.H., Ahmad A.L., (2009), Batch adsorption of phenol onto physiochemical-activated coconut shell, *Journal of Hazardous Materials*, **161**, 1522-1529.

Nguyen A.T., Juang R.-S., (2015), Photocatalytic degradation of p-chlorophenol by hybrid H_2O_2 and TiO_2 in aqueous suspensions under UV irradiation, *Journal of Environmental Management*, **147**, 271-277.

Nourmoradi H., Avazpour M., Ghasemian N., Heidari M., Moradnejadi K., Khodarahmi F., Javaheri M., Moghadam F.M., (2015), Surfactant modified montmorillonite as a low cost adsorbent for 4-chlorophenol: Equilibrium, kinetic and thermodynamic study, *Journal of the Taiwan Institute of Chemical Engineers*, **59**, 244-251.

Saharan V.K., Pinjari D.V., Gogate P.R., Pandit A.B., (2014), *Advanced Oxidation Technologies for Wastewater Treatment: An Overview*, In: *Industrial Wastewater Treatment, Recycling and Reuse*, Ranade V.V., Bhandari V.M. (Eds.), Elsevier, 141-191.

Wang M., Fang G., Liua P., Zhou D., Ma C., Zhang D., Zhan J., (2016), Fe_3O_4@β-CD nanocomposite as heterogeneous Fenton-like catalyst for enhanced degradation of 4-chlorophenol (4-CP), *Applied Catalysis B: Environmental*, **188**, 113-122.

Wang N., Zheng T., Zhang G., Wang P., (2016), A review on Fenton-like processes for organic wastewater treatment, *Journal of Environmental Chemical Engineering*, **4**, 762-787.

Weber W.J., Morris J.C., (1963), Kinetics of adsorption on carbon from solution, *Journal of the Sanitary Engineering Division*, **89**, 31-59.

Xu J.-H., Gao N.-Y., Deng Y., Xia S.-Q., (2013), Nanoscale iron hydroxide-doped granular activated carbon (Fe-GAC) as a sorbent for perchlorate in water, *Chemical Engineering Journal*, **222**, 520-526.

Yao Y., Wang L., Sun L., Zhu S., Huang Z., Mao Y., Lu W., Chen W., (2013), Efficient removal of dyes using heterogeneous Fenton catalysts based on activated carbon fibers with enhanced activity, *Chemical Engineering Science*, **101**, 424-431.